Regular article

Marcin Michałowski*

Simulation model for frictional contact of two elastic surfaces in micro/nanoscale and its validation

https://doi.org/10.1515/ntrev-2018-0075
Received April 19, 2018; accepted August 20, 2018

Abstract: A numerical model is suggested and validated for simulating frictional forces between two samples. The model employs knowledge of surface topographies and values of surface properties provided in the relevant literature and can be applied to contact between complex surfaces. It employs the Lennard-Jones molecular force theory and applies it to a surface segmented into cuboids, which represent separate springs in a Winkler layer. In order to model a contact of two rough surfaces, their asperities are merged into one surface that is put into contact with a perfectly flat surface. Validation, done by atomic force microscopy (AFM), shows that the model can be applied for contacts of rigid samples in the elastic regime of forces.

Keywords: atomic force microscopy; friction; simulation.

Abbreviations: AFM, atomic force microscopy; LPCVD, low-pressure chemical vapor deposition; MEMS, microelectromechanical systems; NEMS, nanoelectromechanical systems

1 Introduction

Reliability is always a significant issue in micro- and nanoelectromechanical systems (MEMS and NEMS). Because of scaling effects, volumetric properties of MEMS/NEMS are not the main focus of failure mode analysis [1–6]. In microscale, surface properties and surface-surface contact mostly affect performance and reliability [7]. Adhesion of surfaces and friction between two sliding surfaces result in stiction (sometimes permanent due to low elastic restoring forces) and wear of mechanisms [8–10]. Adhesion of two surfaces can be modeled based on contact theories such as the Johnson, Kendall, and Roberts (JKR) [11] or Maugis model [12]. With detailed knowledge of both contacting surface topographies, it is possible to predict the adhesion forces between them [13]. Prediction of friction is, however, a more complex issue, and even the measurement of friction forces between two surfaces in microscale is a difficult task [14]. That leads toward a need to develop a way to accurately simulate friction contact of two surfaces. A respective contact model was suggested and validated in this paper.

Previously developed friction models present accurate predictions within limited areas. For example, the Greenwood-Wiliamson statistical approach with Weibull distribution [15] is a good predictor of contact between two surfaces with very limited number of contacting asperities, which comes to very rough surfaces under low loads. Those limitations make it hard to use this model while developing contact surfaces in MEMS and NEMS for minimal friction. There are also models for specific situations such as numerical simulations of rigid body dispersions, which predict frictional behavior during dispersion in solvents [16]; however, they are not applicable to this scale. Molecular dynamics models are also a possibility for predicting contact, but their complexity is still very high. Numerous parameters affect those models, and due to still high error of the results and long computation time, these models still need significant work in order to be applied to the design of MEMS/NEMS devices [17, 18]. Validation of friction models is also a complex task as it might require development of special apparatus to accurately measure nanoscale contact [19]. However, it is possible to use atomic force microscope (AFM) to measure contact parameters with high accuracy, as it was done for other types of simulation models [20–22].

2 Simulation model

In this simulation, the Tabor's theory [23], developed further by McClelland [24], is assumed to be a good

***Corresponding author: Marcin Michałowski,** Faculty of Mechatronics, Institute of Micromechanics and Photonics, Warsaw University of Technology, Boboli 8, 02-525 Warsaw, Poland, e-mail: m.michalowski@mchtr.pw.edu.pl.
http://orcid.org/0000-0002-6946-6840

description of two contacting surfaces. This theory suggests that friction can be divided into adhesive friction and mechanical friction. The adhesive part is caused by molecular bonds between atoms of two surfaces moving relatively to each other. The mechanical part, also called load-controlled or deformation component, describes the force needed for those surfaces to deform each other. Another assumption taken in this model is a simplification of elastic deformation by considering the material as a set of parallel springs as in the Winkler mattress model. Each spring in the Winkler layer is a separate point in the simulation approximating area S. Asperities of two contacting surface topographies are summed to form one rough surface (Figure 1), which is in contact with a flat surface. Additionally, the flat sample is assumed to be rigid, and the Young's modulus of the rough surface is calculated according to Eq. (1) [25].

$$E = \frac{1}{\frac{(1-\nu_1^2)}{E_1} + \frac{(1-\nu_2^2)}{E_2}} \tag{1}$$

where E_1, E_2, ν_1, ν_2 are Young's modulus and Poisson's ratio of material surfaces 1 and 2, respectively.

Deformation of the elastic layer can be derived from the force equilibrium Eq. (2):

$$\sum_{i=1}^{m} P_i(\Delta z_i) + \sum_{i=1}^{n} F(l_i) = N \tag{2}$$

where P_i is the contact deformation force acting on the surface layer deforming it elastically over Δz_i [26]. $F(l_i)$ is the molecular force described by the Lennard-Jones theory, l_i is the distance between the two surfaces in point i and can be described as $l_i = d - z_i$. N is the external force, m is the number of springs being in mechanical contact, and n is the number of springs in strictly adhesive contact. The elementary force opposing the elastic deformation can be described as [26]:

$$P_i(\Delta z_i) = \frac{E}{kh}\Delta z_i \tag{3}$$

where h is the height of the Winkler's layer, and k is:

$$k = \frac{(1+\sqrt{\nu_1\nu_2})\cdot(1-2\sqrt{\nu_1\nu_2})}{1-\nu_1\nu_2} \tag{4}$$

The molecular force $F(l_i)$ can be derived from the Lennard-Jones potential energy equation [27]:

$$E_p = \frac{A}{l_i^n} - \frac{B}{l_i^m} \tag{5}$$

Powers n and m are taken as 2 and 8 due to the assumption of two half-spaces interacting with each other [28]. Afterward, we differentiate Eq. (5) with respect to distance and calculate constants A and B assuming that the force equals 0 when the distance is ε and the adhesion energy to be equal to the integral of the force with respect to the distance over ε to ∞.

$$\Delta\gamma = \int_{\varepsilon}^{\infty} F(l_i)\,dl \tag{6}$$

After these transformations, the force can be calculated as:

$$F(l_i) = \frac{8}{3}\frac{\Delta\gamma}{\varepsilon}\left(\left(\frac{\varepsilon}{l_i}\right)^3 - \left(\frac{\varepsilon}{l_i}\right)^9\right) \tag{7}$$

where ε is the intermolecular distance at which potential energy is minimal, $\Delta\gamma$ is the adhesion energy equal to $\Delta\gamma = \sqrt{\gamma_1\gamma_2}$, where γ_1 and γ_2 are surface energies of samples 1 and 2. For points with no initial mechanical contact $l_i > \varepsilon$, we can calculate the deformation of the elastic layer by assuming a force equilibrium $F(l_i) = P_i(\Delta z_i)$ and using Eqs. (3) and (7),

$$\Delta z_i = \frac{8}{3E}\Delta\gamma kh\left(\frac{\varepsilon^2}{(d-z_i)^3} - \frac{\varepsilon^8}{(d-z_i)^9}\right) \tag{8}$$

where d is the distance between the flat surface and the base of the rough surface, and z_i is the height of the asperity at point i from the base level, as can be seen in Figure 2.

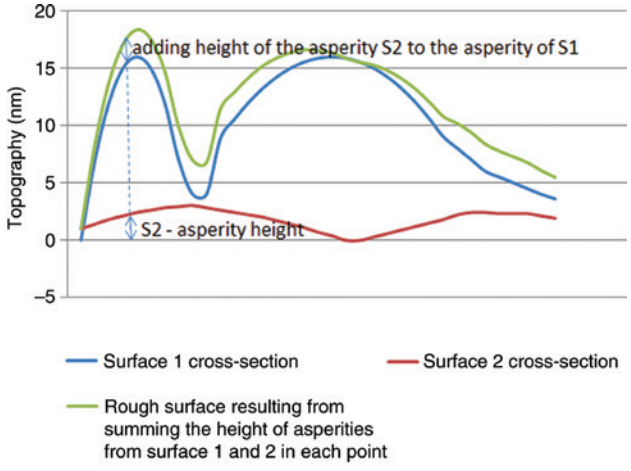

Figure 1: An example of a rough surface used for simulation, modeled in contact with a perfectly smooth surface. This rough surface is created by summing of the asperities of two real surfaces into one.

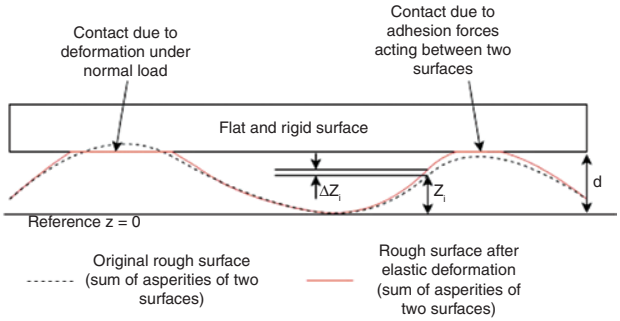

Figure 2: Schematic of contact between two real surfaces. Asperities of two real surfaces are merged into one surface called "rough surface", and the second is presumed to be ideally "flat and rigid surface". The figure shows deformation of the "rough surface" under load and due to adhesion forces.

Each spring in the model is a cuboid of the surface material with its height being the height of the Winkler's layer and its upper area is equal to S. When two surfaces: "rough surface" and "flat and rigid surface" are moving laterally with respect to each other, each cuboid is sheared. A schematic of a sheared element is shown in Figure 3. The work of the shear force is:

$$W = \frac{1}{2} Q_i \Delta s_i \tag{9}$$

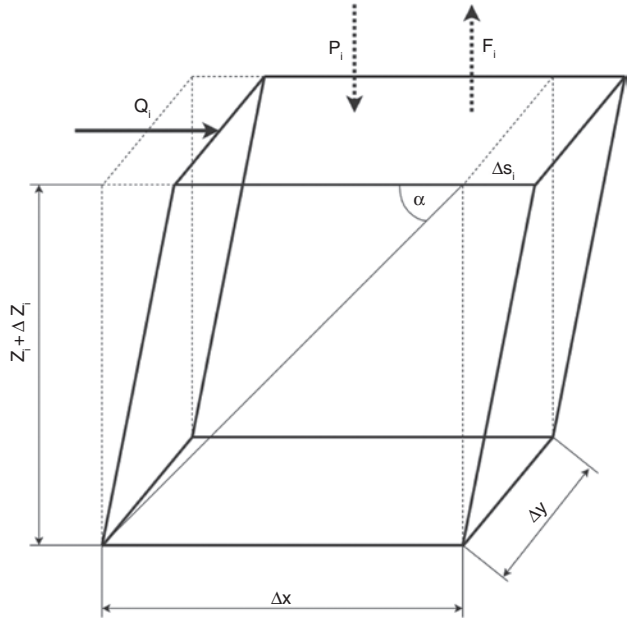

Figure 3: With a surface modeled as collection of parallel springs, one spring representing a cuboid of the surface material is shown. Δx and Δy are the dimensions of the cuboid in this model, assumed to be the size of the step set during surface topography measurement. Z_i is the height of the layer, Q is the shearing force, while P and F are the load and adhesion forces that could stretch or compress z_i.

An extension of the diagonal of the cuboid resulting from the shear can be calculated in two ways. Strictly geometrical under an assumption that the angle between the diagonal and the top side (α in Figure 3) does not change with the shear of the top, due to a low deformation of the cuboid:

$$\Delta l = C \cdot \frac{\Delta s_i}{z_i + \Delta z_i} \tag{10}$$

where $C = \frac{\tan\alpha}{\tan^2\alpha + 1}$, $\tan\alpha = \frac{z_i + \Delta z_i}{\Delta x}$, Δx is the side of the upper square of the cuboid.

The second way of denoting an extension is to use a well-known equation, due to stretching of the material in the direction and contracts in the direction traverse of the stretching:

$$\Delta l = \frac{\sigma_1}{E} - \nu \frac{\sigma_2}{E} \tag{11}$$

where $\sigma_1 = \frac{Q}{S}$, and $\sigma_2 = -\frac{Q}{S}$.

From Eqs. (10) and (11), we can calculate:

$$\Delta s_i = \frac{Q_i}{2CGS}(z_i + \Delta z_i) \tag{12}$$

where $G = \frac{E}{2(1+\nu)}$, S is the upper surface area of one calculated cuboid. Substituting Eq. (12) into Eq. (9), we get an equation for work of the shear force:

$$W = \frac{1}{4} Q_i^2 (z_i + \Delta z_i) \frac{1}{CGS} \tag{13}$$

The energy needed to break contact can be derived from Eq. (7) by assuming the separation of surfaces from distance l_{ia} to ∞

$$En = \int_{l_{ia}}^{\infty} \frac{8\Delta\gamma}{3\varepsilon} \left(\left(\frac{\varepsilon}{l_i} \right)^3 - \left(\frac{\varepsilon}{l_i} \right)^9 \right) dl_i = \frac{8\Delta\gamma}{3} \cdot \left(\frac{\varepsilon^2}{2l_i^2} - \frac{\varepsilon^8}{8l_i^8} \right) \tag{14}$$

where $l_{ia} = d - (z_i + \Delta z_i)$.

Assuming that the work of the shear force has to be equal to the energy needed to break contact, we can use Eqs. (13) and (14) to calculate the lateral force needed to destroy the adhesion bonding at point i:

$$Q_i = \left(\frac{1}{z_i + \Delta z_i} 4CGS \int_{l_{ia}}^{\infty} \frac{8\Delta\gamma}{3\varepsilon} \left(\left(\frac{\varepsilon}{l_i} \right)^3 - \left(\frac{\varepsilon}{l_i} \right)^9 \right) dl_i \right)^{\frac{1}{2}}$$

$$= \left(\frac{1}{z_i + \Delta z_i} 4CGS \cdot \frac{8\Delta\gamma}{3} \cdot \left(\frac{\varepsilon^2}{2l_i^2} - \frac{\varepsilon^8}{8l_i^8} \right) \right)^{\frac{1}{2}} \tag{15}$$

The lateral force is summed for all points, where adhesive contact occurs. The contact component is calculated using the previously determined force P_i. Knowing the external force N, it is possible to calculate the distance d from Eq. (2) and then P_i from Eq. (3). Then, we can calculate the distance l_{im} at which the molecular force $F(l_i)$ is equal to P_i. Afterward, the energy needed to break contact is calculated as the energy needed to separate the initial contact from the distance l_{im} to ε and from that point to ∞. The calculation of energy needed is similar to that of Eq. (14).

$$Enm = \int_{l_{im}}^{\infty} \frac{8\Delta\gamma}{3\varepsilon}\left(\left(\frac{\varepsilon}{l_i}\right)^3 - \left(\frac{\varepsilon}{l_i}\right)^9\right) dl_i \tag{16}$$

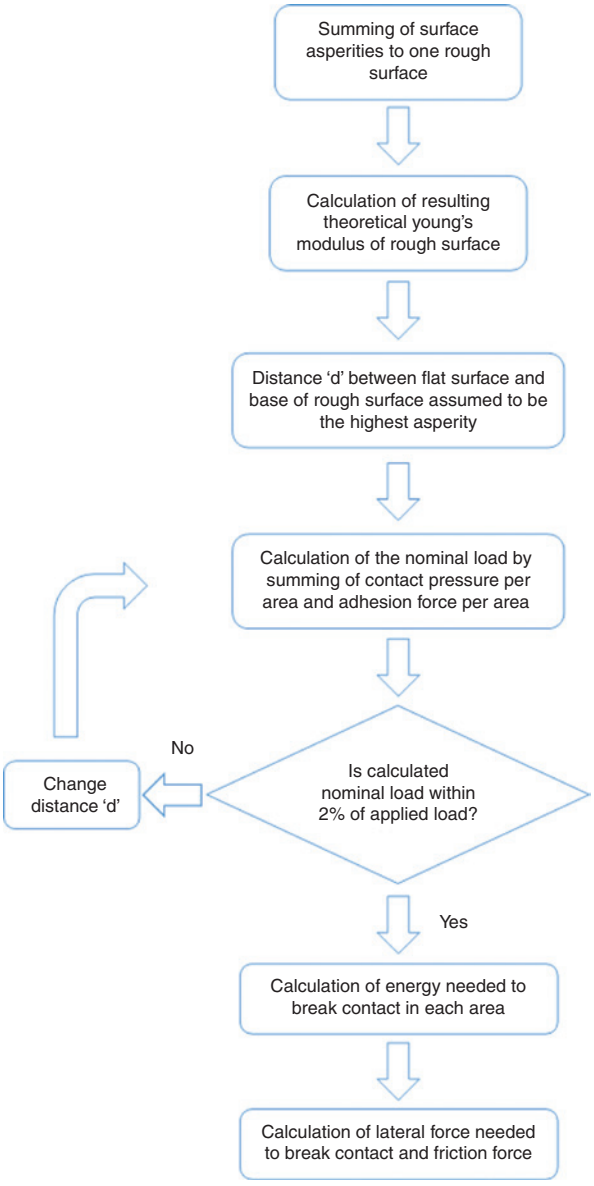

Figure 4: Block schematic of the friction simulation algorithm.

The lateral force needed to break the contact can be calculated in a similar way as Eq. (15):

$$Q_i = \left(\frac{1}{d} 4CGS \int_{l_{im}}^{\infty} \frac{8\Delta\gamma}{3\varepsilon}\left(\left(\frac{\varepsilon}{l_i}\right)^3 - \left(\frac{\varepsilon}{l_i}\right)^9\right) dl_i\right)^{\frac{1}{2}} \tag{17}$$

The force required to separate a contact is summed for every cuboid in the model, both while in contact due to the deformation of the surface under normal load and while in contact due to adhesion forces.

It is also possible to calculate those values for a situation, where the two contacting surfaces were held in contact for some time prior to movement by assuming a time-dependent elastic modulus [29]. This model for the time being was implemented in Delphi; however, owing to a fairly simple algorithm (Figure 4), it can be transferred to other programming languages.

3 Simulation studies

In order to simulate the contact of two surfaces with this method, some parameters of the samples have to measured or assumed. In the model, we assume the intermolecular distance ε to be 2 nm [27] and the Winklers layer thickness as the thickness of the measured layer. The area of a single spring in the model is important as well; it was assumed to be the step of scanning during the AFM measurement of the surface, which was 20 nm×20 nm. The AFM was used because it is a widely available and commonly used instrument [30–34]. This could allow for an easy acquisition of model inputs.

Other inputs of the model are surface free energy of samples, elastic modulus, and Poisson's ratio of both materials and detailed topography of surfaces.

3.1 Validation method

The validation of the model was done by assuming one of the contacting surfaces to be a sphere sliding over a flat surface (Figure 5). Because of this assumption, the outputs of the model can be compared with the AFM friction loop measurements. A cantilever with a spherical tip was used on various samples to measure the lateral force and, as the result, the coefficient of friction. One additional simplification was added at this point: the tip sphere was not modeled as a whole sphere, but rather

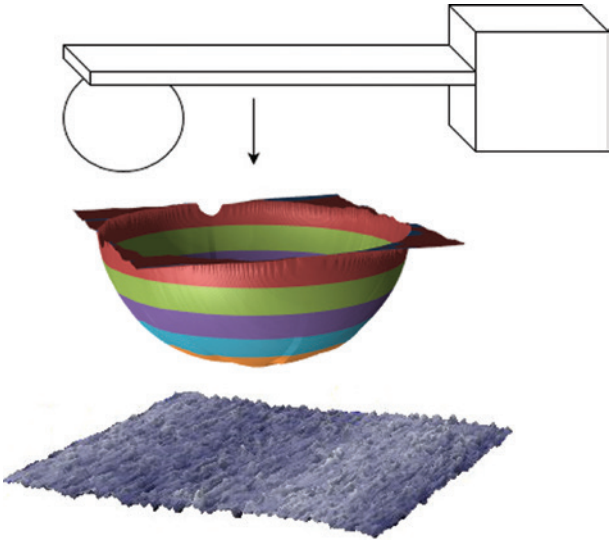

Figure 5: Schematics of the simulation validation method. A spherical surface that comes into contact with the sample is moved laterally. The spherical surface in the experiment is a cantilever tip; from the top, we can see a cantilever with a spherical tip; part of the sphere used to calculate the contact; polysilicon sample surface (with 20:1 ratio in the axis z with respect to x and y).

as a half sphere. During the test, no sample with roughness higher than 70 nm Ra was used; therefore, the force between the higher parts of the sphere and the surface sample are negligible. As the exact point of initial contact will, in most cases, not be known in nanometer resolution, validation was done by numerous measurements of topography and friction on the same samples but over different areas, and averaging of both values: measurement of friction and simulated friction for multiple sample surface with the AFM tip.

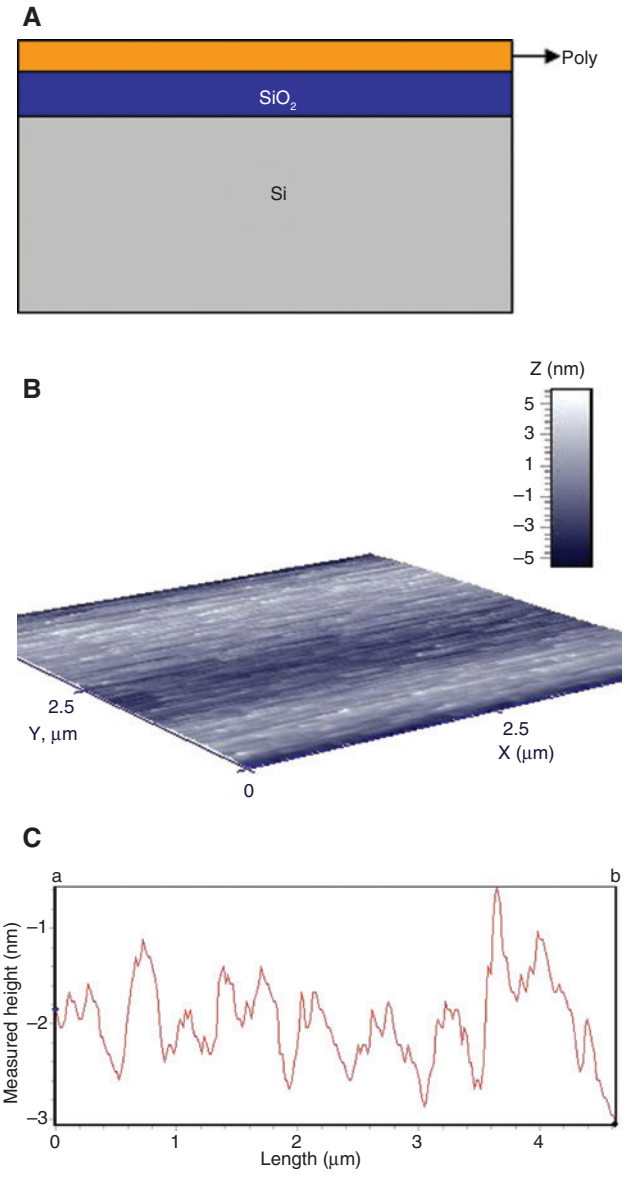

Figure 6: Silicon samples measured during validation of the model. (A) Cross section of the silicon sample layers (not to scale). (B) Sample topography. (C) Sample topography cross section.

4 Measurements

In order to validate the model, a cantilever with a SiO_2 tip with a diameter of 2 µm was used. This cantilever was CP-NCH-SiO-A from sQube. Calibration of the cantilever in the z axis was realized by a reference spring with a stiffness of 35.5 N/m and the Si wafer as the hard material for photodiode calibration [35]. In the torsional axis, the calibration was done on the basis of the measurements of the geometrical dimensions of the beam and the assumption of the AFM manufacturer that photodiode sensitivity is equal in both directions. An NT-206 AFM system was used during this study. Friction loop measurements were done on polysilicon samples (Figure 6) produced by low-pressure chemical vapor deposition (LPCVD) with different deposition temperatures, by thermal decomposition of silane in temperatures of 580°C, 610°C, and 630°C. Layers were produced on SiO_2, which was attained through thermal oxidation of <100> -oriented silicon substrate. The SiO_2 film thickness manufactured in that way was 1.7 µm. Various temperatures of polysilicon deposition resulted in change in the roughness and the grain size of the top layer. The duration of the deposition was controlled in order to achieve a constant thickness of the polysilicon layer of 50 nm for all samples.

The topography of both cantilever tip and samples was measured by the AFM with a step of data acquisition

of 20 nm × 20 nm, using a sharp tip CSC17-No Al-15 from MikroMasch. The topography was measured in contact mode with low loads. For polysilicon samples, the measurements were done over an area of 5 μm × 5 μm at seven separate spots. No significant deformations or differences were spotted between scans. Additionally, scans over a larger area of 20 μm × 20 μm were done to check if larger deformations exist on the surface of the sample. In the case of the spherical tip CP-NCH-SiO-A, its topography was acquired by repeated scans on the AFM and combining the resulted areas.

Young's modulus of the polysilicon samples was measured on a Tryboscope using the indentation procedure with the application of the Oliver and Pharr model [36]. For these measurements, the Berkovitch tip was used. A trapezoidal loading curve with both loading and unloading time of 5 s and a holding time of 2 s was used. The maximum load during those measurements was 1500 μN. In order to avoid the impact of the substrate during the measurements, samples with a 2-μm polysilicon layer were prepared utilizing the same fabrication process. The value obtained was 110 GPa. During this study, a Hysitron Tryboscope was used. For the purpose of simulation, it was accepted that the Young's modulus of SiO_2 is 70 GPa, according to Ref. [37]. For both samples, literature values of Poisson's ratio were used: 0.22 [38] for polysilicon and 0.17 [37] for SiO_2, respectively.

Surface free energy of the LPCVD-prepared samples was measured according to a wettability method [39]. Five microliters of droplets of water and diiodomethane were placed on samples, and their angle with the surface was measured. Afterward, the surface free energy of the samples was calculated [39]. Because of the spherical shape of the cantilever, the wettability procedure was not used for the cantilever tip; in this case, a value of 72 mJ/m^2 [40] was used in the model.

Friction loop measurements with the use of the simulated cantilever were done on each of these samples seven times at various locations on the sample, and the average value was accepted to be compared with the simulation results. The friction measurements were done under a constant load of 10 μN and a sliding speed of 3.5 μm/s. The constant load was achieved by a feedback loop system with the AFM piezo-element controlling the deflection of the cantilever to be constant at the level at which 10 μN load is exacted on the surface. A 10-μN load was selected in order to be certain that the contact stays in the elastic regime. The Hertz contact model for a ball with 2 μN in contact with a flat surface for these materials shows that in order to exceed the polysilicon yield strength, a load of 70 μN would have to be applied. Kinematic friction was used for comparison with the simulation. The measurement devices and example results are depicted in Figure 7. All of these measurements were done

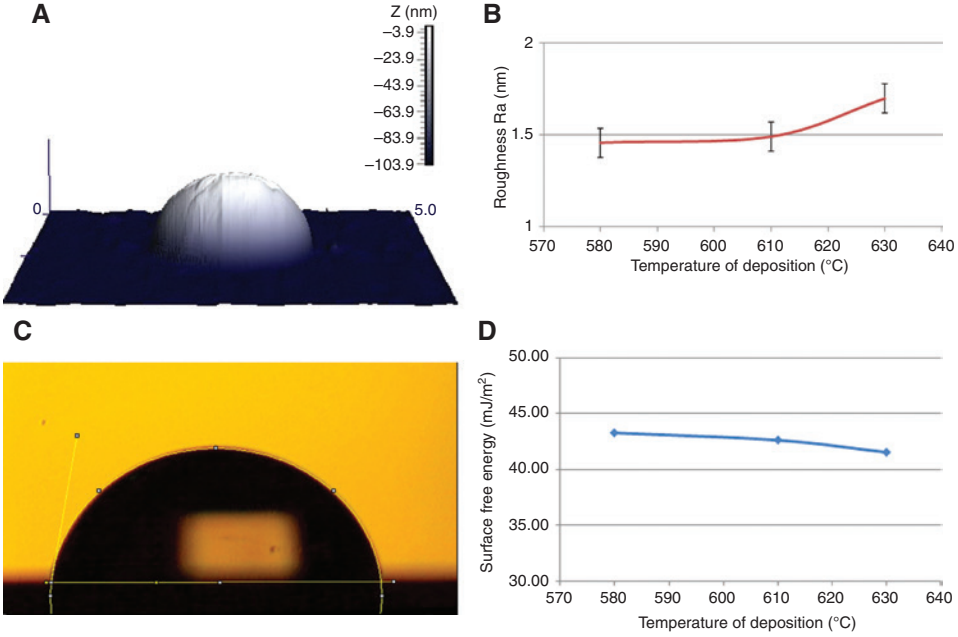

Figure 7: Example of the measurement results. (A) Cantilever tip surface. (B) Roughness of the polysilicon samples. (C) Example of a water droplet on a polysilicon sample. (D) Surface free energy of polysilicon samples.

in a clean room with controlled environment, with a temperature of 22.3°C and a humidity of 53.1–56.2%.

5 Results

In the simulated samples, the adhesive component of friction is dominating the mechanical part and is roughly 40 times greater for all the SiO_2-polysilicon contacts. In both friction measurements and simulation, the same normal load of 10 μN was applied; therefore, the comparison of the friction coefficient is equivalent to the comparison of the lateral force. The average values of the friction coefficient from seven measurements and from seven simulations, one for each topography scan of polysilicon in contact with the cantilever plane, are depicted in Figure 8.

A two-sample t-test was done on each surface pair resulting in p values of 0.13, 0.12, and 0.79 for roughness values of 1.45, 1.49, and 1.7 μm; each of these values is greater than the assumed threshold of 0.1. Additionally, the R-Pearson correlation between averages was calculated to be 0.96, which is a high strength correlation. Simulation is in line with the measurements giving a good prediction of the values.

Figure 9 depicts the range of friction coefficient values for each simulation compared to the range of values obtained from the measurements. We can see that the scatter of both simulation and experimental values is similar, which further suggests the accuracy of the model.

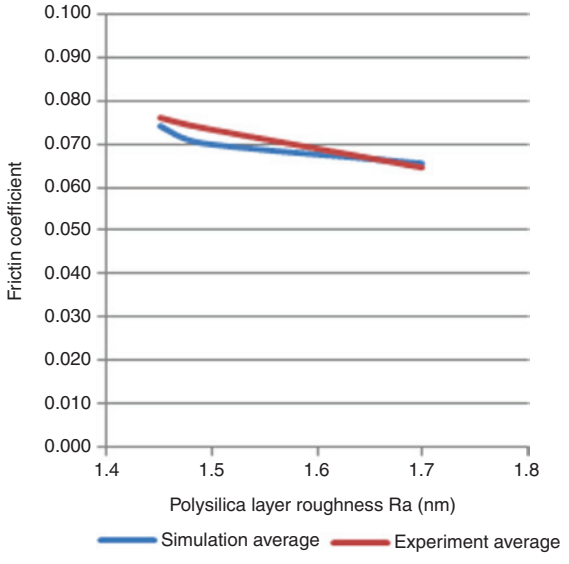

Figure 8: Comparison of the coefficient of friction of SiO_2 friction with polysilicon samples of varied roughness, from simulation and experiment.

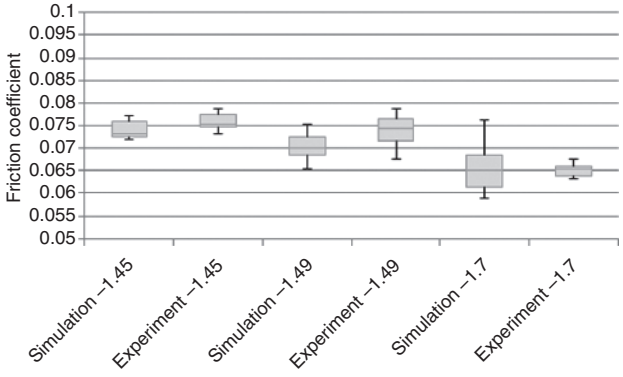

Figure 9: Box plots of simulation and experimental values of SiO_2 and polysilicon contact showing the dispersion range of results, for varied roughness of polysilicon. Boxes denote the range between 1 and 3 quartile, while the whiskers show the range between the minimum and maximum value.

6 Discussion

The simulation model is a good predictor for contacts of two smooth samples. The influence of change in roughness of one surface on the friction is predicted accurately. At this point, the model is accurate for contact between samples when the adhesion contact is dominant as no mechanical locking of two surfaces is taken into account. The adhesive part of friction will be greater than the mechanical one for smooth samples and during low loads. For example, for a simulated sample (Ra of 1.7 nm) in contact with the 2-μm diameter ball tip, the mechanical part exceeds the adhesive part at about 600 μN of load. This model assumes the surface to consist of cuboids with x and y dimensions according to the scan size. This assumption has a negligible effect on smooth surfaces, but surfaces with higher kurtosis, with more spiked asperities, will be affected more by this simplification. By assuming the top of the asperity to be a cuboid of x,y dimensions instead of a sharp end, the contact area will be significantly overestimated at this point, resulting in overestimation of the force needed to break contact, which in turn overestimates the friction force. This was tested on samples with higher roughness and kurtosis (Ra ~50 nm and Rku ~3), and the step of data acquisition for topography had to be 5 nm × 5 nm or less to correctly simulate the friction force. As this model is meant to be used in conjunction with the topography measured by the AFM, which scans the

sample in particular points and not the highest points of the asperities, the flat cuboid should be statistically indistinguishable from the actual surface for a small-enough measuring mesh. One more noteworthy limitation of the model is that it assumes an elastic contact and no plastic deformation. That means that simulation is only accurate when loads do not exceed the elastic regime of the measured surface material. This limitation is, however, met for majority of the loads existing in MEMS/NEMS and materials such as polymers, silicon, silicon dioxide, or polysilicon [41, 42]. Calculation of friction based on topography and more easily measured properties such as surface free energy can lead toward easier prediction of surface interaction than either uncertain off-chip measurement methods or expensive and time-consuming on-chip measurements [43].

7 Summary

A simulation model for the contact of two surfaces is discussed. The model allows the prediction of friction forces with the separation for adhesion friction and mechanical friction. The model uses the Winkler's layer model, Lennard-Jones energy of contact, and Tabor's friction theory as its base. This is a numerical model with a simulation step size possible to be set according to the resolution, with which we measured the simulated surfaces. The inputs of the model are both surface topographies, and their properties such as elasticity, surface free energy, and Poisson's ratio. Simulation outputs were validated for smooth surfaces in which the adhesive part of the friction is dominant. Further validation of rough samples and plastic range of deformation are required to specify the exact range of model application. It is planned to continue the validation of other materials in order to confirm the effects of surface energy and elastic properties on friction results, to ensure accurate prediction over a wide range of values. The proposed model is simpler and faster in calculation than the molecular dynamics models and can be applied to highly patterned surfaces of elements within the elastic regime. The prediction of friction forces in MEMS and NEMS devices can possibly lead toward a more optimized development of NEMS actuators.

Acknowledgments: The author would like to thank Sergiusz Łuczak, D.Sc. Ph.D. Eng., for the critical revision of the manuscript.

References

[1] Sniegowski JJ, Miller SL, LaVigne G, Rodgers MS, McWhorter PJ. Monolithic geared-mechanisms driven by a polysilicon surface-micromachined on-chip electrostatic engine, In *Technical Digest of the 1996 Solid State Sensor and Actuator Workshop*, Hilton Head Island, SC, June 3–6, 1996, pp. 178–182.

[2] Rodgers MS, Sniegowski JJ, Miller SL, Barron CC, McWhorter PJ. Advanced micromechanisms in a multi-level polysilicon technology. In *SPIE Micromachined Devices and Components III*, Austin, TX, September 29, 1997, 3224. pp. 120–130.

[3] Miller SL, LaVigne G, Rodgers MS, Sniegowski JJ, Waters JP, McWhorter PJ. Routes to failure in rotating MEMS devices experiencing sliding friction. In *Proc. SPIE Micromachined Devices and Components III*, Austin, September 29, 1997, 3224, pp. 24–30.

[4] Komvopoulos K. Surface engineering and microtribology for micromechanical systems. *Wear* 1996, 200, 305–327.

[5] Romig A, Dugger M, McWhorter P. Materials issues in microelectromechanical devices: science, engineering, manufacturability and reliability. *Acta Mater.* 2003, 51, 5837–5866.

[6] Alsem D, van der Hulst R. Wear mechanisms and friction parameters for sliding wear of micron-scale polysilicon sidewalls. *Sens. Actuat. A* 2010, 163, 373–382.

[7] Miller SL, Rodgers MS, La Vigne G, Sniegowski JJ, Clews P, Tanner DM, Peterson KA. Failure modes in surface micromachined microelectromechanical actuation systems. *Microelectron. Reliab.* 1999, 39, 1229–1237.

[8] Smallwood S, Eapen K, Patton S, Zabinski J. Performance results of MEMS coated with a conformal DLC. *Wear* 2006, 260(11–12), 1179–1189.

[9] Tanner D, Miller W, Eaton W, Irwin L, Peterson K, Dugger M, Senfit D, Smith N, Tangyunyong P, Miller S. The effect of frequency on the lifetime of a surface micromachined microengine driving a load. In *IEEE Reliability Physics Symposium Proceedings*, 26–35, 1998.

[10] Zhanshe G, Yonggang M, Hao W, Caijun S, Shizhu W. Measurement of static and dynamic friction coefficient of sidewalls of bulk-microfabricated MEMS devices with an on-chip microtribotester. *Sens Actuat. A Phys.* 2007, 135, 863–69.

[11] Johnson K, Kendall K, Roberts A. Surface energy and the contact of elastic solids. *Proc. Roy. Soc. London A* 1971, 324, 301.

[12] Maugis D. Adhesion of spheres: the JKR-DMT transition using a dugdale model. *J. Colloid Interface Sci.* 1992, 150, 243.

[13] Prokopovich P. Adhesion models: from single to multiple asperity contacts. *Adv. Colloid Interface Sci.* 2011, 168(1–2), 210–222.

[14] Tang XS, Loke YC, Lu P, Sinha SK, O'Shea SJ. Friction measurement on free standing plates using atomic force microscopy. *Rev. Sci. Instrum.* 2013, 84, 013702.

[15] Lu P, O'Shea S. Mechanical contact between rough surfaces at low load. *J. Phys. D: Appl. Phys.* 2012, 45(47), ID 475303.

[16] Molina J, Yamamoto R. Direct numerical simulations of rigid body dispersions. I. Mobility/friction tensors of assemblies of spheres. *J. Che. Phys.* 2013, 139(23). doi: 10.1063/1.4844115.

[17] Dong Y, Li Q, Martini A. Molecular dynamics simulation of atomic friction: a review and guide. *J. Vac. Sci. Technol. A* 2013, 31(3), ID 30801.

[18] Ye Z, Martini A. Atomic friction at exposed and buried graphite step edges: experiments and simulations. *Appl. Phys. Lett.* 2015, 106(23), 231603–231603.5.
[19] Qing T, Shao T, Wen S. Micro-friction and adhesion measurements for Si wafer and TiB2 thin film. *Tsinghua Sci. Technol.* 2007, 12(3), 261–268.
[20] Korayem MH, Kavousi A, Ebrahimi N. Dynamic analysis of tapping-mode AFM considering capillary force interactions. *Sci. Iran.* 2011, 18(1), 121–129.
[21] Korayem MH, Zakeri M. Dynamic modeling of manipulation of micro/nano particles on rough surfaces. *Appl. Surf. Sci.* 2011, 257(15), 6503–6513.
[22] Korayem MH, Sadeghzadeh S, Rahneshin V. A new multiscale methodology for modeling of single and multi-body solid structures. *J. Comput. Mater. Sci.* 2012, 63, 1–11.
[23] Tabor D. The role of surface and intermolecular forces in thin film lubrication. *Tribol. Ser.* 1982, 7, 651–682.
[24] McClelland GM. Friction at weakly interacting interfaces. In *Adhesion and Friction*, Grunze, M, Kreuzer, HJ, Eds., Springer: Berlin, Heidelberg, 1989, pp. 1–16.
[25] Chen R-H, Weng Y-J, Hurng H-Y, Wang Y-L, Tsai C-T. Study of transfer printing using micro-dynamically-regulated microstructural flexible mold. *Optik – International Journal for Light and Electron Optics* 2016, 127(7), 3590–3596.
[26] Johnson K. *Contact Mechanics*, Cambridge University Press: Cambridge, UK, 1985.
[27] Azoroff L. *Introduction to Solids*, Mc Graw-Hill: New York, 1960.
[28] Israelachvili J. *Intermolecular and Surface Force*, Elsevier: Cambridge, 2011.
[29] Nolbert D, Rymuza Z. Modelling of frictional and adhesive contacts at silicon/polymer interface for nanotechnological applications. *Tribology – Mater. Surf. Interfaces* 2013, 7(2), 97–102.
[30] Jarząbek D, Kaufmann A, Schift H, Rymuza Z, Jung T. Elastic modulus and fracture strength evaluation on the nanoscale by scanning force microscope experiments. *Nanotechnology* 2014, 25, 215701-1–9.
[31] Abetkovskaya S, Chizhik S, Pogoskaya I, Rymuza Z, Jarząbek D, Michalowski M, Linke J. Determining the Young modulus of nanosize thickness coatings for MEMS from the results of static force spectroscopy. *Bull. Russ. Acad. Sci. Phys.* 2012, 76(9), 1009–1011.
[32] Kucharski S, Jarząbek D, Piątkowska A, Woźniacka S. Decrease of nano-hardness at ultra-low indentation depths in copper single crystal. *Exp. Mech.* 2016, 56(3), 381–393.
[33] Jarząbek D, Siewert D, Fabianowski W, Schift H, Rymuza Z, Jung T. Influence of alkali ions on tribological properties of silicon surface. *Tribol. Lett.* 2015, 60(2), 1–8.
[34] Uchihashi T, Watanabe H, Fukuda S, Schibata M, Ando T. Functional extension of high-speed AFM for wider biological applications. *Ultramiscroscopy* 2016, 160, 182–196.
[35] Sikora A, Bednarz L, Ekwiński G, Ekwińska M. The determination of the spring constant of T-shaped cantilevers using calibration structures. *Meas. Sci. Technol.* 2014, 25(4), ID 044015.
[36] Oliver WC, Pharr GM. Measurement of hardness and elastic modulus by instrumented indentation: Advances in understanding and refinements to methodology. *J. Mater. Res.* Jan. 2004, 19(1), 3–20.
[37] Kim MT, Influence of substrates on the elastic reaction of films for the microindentation tests. *Thin Solid Films* 1996, 283, 12–16.
[38] Sharpe W, Yuan B, Vaidyanathan R, Edwards R. In *Proceedings of the 10th MEMS Workshop*, Nagoya, Japan, 1997, pp. 424–429.
[39] Andersen W. Wettability literature survey – part 2: wettability measurement. *SPE* 1986, 13933, 1246–1258l.
[40] Chibowski E. Surface free energy and wettability of silyl layers on silicon determined from contact angle hysteresis. *Adv. Colloid Interface Sci.* 2005, 113, 121–131.
[41] Greenwood J. Contact of nominally flat surfaces. *Proc. R. Soc. A* 1966, 295, 300–319.
[42] Maugis D. On the contact and adhesion of rough surfaces. *J. Adhes. Sci. Technol.* 1996, 10, 161–175.
[43] Guo Z, Feng Z. Research development of measuring methods on the tribology characters for movable MEMS devices: a review. *Microsyst. Technol.* 2009, 15, 343–354.

Bionote

Marcin Michałowski
Faculty of Mechatronics, Institute of Micromechanics and Photonics, Warsaw University of Technology, Boboli 8, 02-525 Warsaw, Poland, http://orcid.org/0000-0002-6946-6840.
m.michalowski@mchtr.pw.edu.pl

Marcin Michałowski MSc, with a degree from Warsaw University of Technology Department of Mechatronics, is a mechanical engineer with experience in micro- and nano-tribology. His expertise involves friction simulations and measurements, protective coatings, and development of measurement procedures. He is the main organizer of the 8th International Colloquium on Micro-Tribology.